Dalton Transactions

PAPER

View Article Online
View Journal

Cite this: DOI: 10.1039/c3dt52510d

Synthesis, characterization and heterogeneous catalytic application of copper integrated mesoporous matrices†

Swapan K. Das,[a] Sanghamitra Mukherjee,[a] Luís M. F. Lopes,[b] Laura M. Ilharco,[b] Ana M. Ferraria,[b] Ana M. Botelho do Rego[b] and Armando J. L. Pombeiro*[a]

Ordered copper integrated mesoporous silicate catalysts (CuMSC) have been synthesized by the utilization of the amphiphilic tri-block copolymer pluronic F127 as a structure directing agent (SDA) under acidic aqueous conditions. The mesophase of the materials was investigated using small-angle powder X-ray diffraction and transmission electron microscopic (TEM) image analysis. N_2 adsorption–desorption studies show that the BET surface area of CuMSC (214–407 m^2 g^{-1}) is lower than that of pure silica (611 m^2 g^{-1}) and has smaller average pore dimensions (4.0–5.0 nm), both prepared following the same synthetic route. The reduction of pore size and surface area points to incorporation of copper within the silicate network. FEG-SEM results suggest that the materials have a plate-like morphology and are composed of very tiny nanoparticles. EDS surface chemical analysis was utilized for the detection of the distribution of Si, O and Cu in the matrix. The FT IR spectral study suggests the complete removal of the surfactants from the calcined materials and the presence of Si–O–Cu bonds for high nominal contents. X-ray photoelectron spectroscopy (XPS) and UV-vis reflectance spectra show the oxidation state of copper and coordination mode, respectively. These mesoporous materials display a good catalytic activity in the oxidation of cyclohexane to cyclohexanone and cyclohexanol in the presence of the green oxidant hydrogen peroxide. The maximum yield (cyclohexanone and cyclohexanol) was *ca.* 29% and the TON (turnover number) was 276 under optimal reaction conditions. The good catalytic activity could be attributed to the large surface area and the presence of a high number of active sites located at the surface of the material, as well as to its stability. The catalysts showed negligible loss of activity after five cycles.

Received 12th September 2013,
Accepted 27th November 2013

DOI: 10.1039/c3dt52510d

www.rsc.org/dalton

1. Introduction

Mesoporous materials have attracted mammoth interest for the scientific community due to their unique structural and textural features, such as high surface area, large pore volume, and ordered pore networks with uniform and well-defined pore architecture.[1] These features have made them candidates for versatile applications, *e.g.*, gas storage,[2] adsorption/separation,[3] sensors,[4] solar cells,[5] and catalysis.[6,7] As a prototypical mesoporous material, purely siliceous SBA-15 possesses a high surface area and uniform tubular channels with thick pore walls, and offers higher thermal and hydrothermal stabilities than those of MCM-41 with thinner pore walls.[8] All these properties of SBA-15 make it attractive as a more appropriate material for catalytic support.[8,9] Nevertheless, the major limitations of the SBA-15 material concern the few catalytically active sites on its amorphous wall.[10] Thus, it would be desirable to incorporate active sites (metal ions) other than Si^{4+} into the SBA-15 porous framework for its possible use as a catalyst.[11]

Many protocols have been developed to incorporate transition metals, such as bivalent (Cu, Co, Ni, Zn, *etc.*), trivalent (Al, Fe, Ga, *etc.*) or tetravalent (Ti, Zr, Sn, *etc.*) ones, into the mesoporous silicate frameworks.[7,11–15] The direct solvothermal method consists of the direct addition of metal ion precursors to the synthesis gel prior to the treatment.[13,14] Other methods, like wet impregnation and grafting,[7,9,16] face several problems including the loss of the periodic ordering, low metal loadings, or formation of bulk species outside the silica host.[17] Some copper modified silicates are known,[18,19] but they suffer

[a]*Centro de Química Estrutural, Complexo I, Instituto Superior Técnico, Universidade de Lisboa, Av. Rovisco Pais 1, 1049-001 Lisboa, Portugal. E-mail: pombeiro@tecnico.ulisboa.pt; Fax: (+351)-21-846-4455; Tel: (+351)-21-841-9237*

[b]*Centro de Química-Física Molecular and IN – Institute of Nanoscience and Nanotechnology, Instituto Superior Técnico, Universidade de Lisboa, Av. Rovisco Pais 1, 1049-001 Lisboa, Portugal*

†Electronic supplementary information (ESI) available. See DOI: 10.1039/c3dt52510d

limitations like loss of pore ordering, pore blocking, inhomogeneous copper distribution, and formation of bulk species outside the silica host. CuO_x/SBA-15 catalysts have been developed for the selective oxidation of methane.[18b] On the other hand, directly copper doped silicates have been prepared by the hydrothermal method from basic aqueous medium, but with the possible formation of bulk CuO on the silica surface.[19] Very recently, Bhaumik *et al.* have developed copper doped silicates through complexation, and utilized them as catalysts in organic reactions.[7,20]

The oxidation of cyclohexane to cyclohexanol and cyclohexanone is an important challenge from both the academic and industrial viewpoints, since such products are used for the manufacture of adipic acid and caprolactam, which are raw materials for the syntheses of nylon-66′, soaps and detergents, rubber chemicals, pesticides, *etc.*[21,22] Furthermore, cyclohexanone is utilized as an industrial solvent and activator in oxidation reactions. The conventional industrial process for cyclohexane oxidation utilizes Co salt as a homogeneous catalyst and O_2 as an oxidant, at a considerably high temperature (150 °C), and the yield of cyclohexanone is low (*ca.* 4%) to get a good selectivity.[21] Thus, it is important to find out more active systems under milder conditions. Different metal complexes (of V, Cu, *etc.*) show good catalytic activities under homogeneous conditions,[23,24] but heterogeneous catalysts, like transition metal doped silica, have also been developed for this reaction,[22,25,26] offering the usual advantages regarding easy product isolation and catalyst reusability, minimizing the wastage of products during the catalyst separation.[27]

In this context, here we have developed ordered new copper integrated mesoporous silicate catalysts (CuMSC) through the direct addition of a Cu source to the synthesis gel in the presence of a mixture of pluronic F127 and 1,2,4-trivinylcyclohexane (TVCH) under acidic aqueous conditions. Herein, the direct synthesis method involves the matched hydrolysis and condensation rates of silica and Cu precursors, which are essential factors to achieve a stable highly ordered mesoporous architecture. Moreover, suitable adjustment of pH is also crucial to increase the Cu content in the silica framework. Since most of the Cu sources dissolve in strong acids, and the purely siliceous phase of SBA-15 like materials is usually synthesized in strongly acidic media (2 M HCl solution), the incorporation of Cu into the SBA-15 framework by direct synthesis is hampered.[8] To the best of our knowledge, the fabrication of a CuMSC with a large pore dimension by using pluronic F127 as a structure directing agent (SDA) through the hydrothermal method and its use as a heterogeneous solid acid catalyst in cyclohexane oxidation have not been explored so far. In most of the cases, mesoporous CuMSC and other related oxidation catalysts have been synthesized mainly through the post-synthesis method. Furthermore, in the catalysts prepared by this method, the active sites are not easily accessible to the reactants due to pore blocking, and the distribution of active sites is inhomogeneous leading to a low reactivity.

Here, we have synthesized in a single pot, by using the direct synthesis method, a CuMSC with ~5.0 nm and high surface area that reduces the probability of pore blocking and the inhomogeneity problem. The high surface area together with the large pore and accessible active sites of the CuMSC facilitates the oxidation of cyclohexane to cyclohexanone and cyclohexanol. These catalysts were characterized using powder XRD, TEM, SEM-EDS, XPS, N_2 sorption, UV-visible reflectance and FT IR spectroscopy.

2. Experimental section

2.1. Chemicals

The non-ionic triblock copolymer poly(ethylene glycol)-*block*-poly-(propylene glycol)-*block*-poly(ethylene glycol) (pluronic F127, M_{av} = 12 600, $EO_{106}PO_{70}EO_{106}$) was used as the structure-directing agent (SDA), 1,2,4-trivinylcyclohexane was used as a co-surfactant, and tetraethyl orthosilicate (TEOS), bis-[3-(triethoxy silyl)propyl]tetrasulfide (TESPTS) and cuprous iodide (CuI) were used as the silica and copper sources, respectively. These compounds, as well as cyclohexane, cyclopentanone, hydrogen peroxide (H_2O_2) and potassium chloride (KCl), were purchased from Sigma-Aldrich. Hydrochloric acid (HCl, 37 wt%, Riedel-de-Haën), nitric acid (65 wt%, Riedel-de-Haën), acetonitrile (MeCN, Riedel-de-Haën) and triphenylphosphine (Merck) were also purchased from commercial sources. Here, HCl and KCl were utilized to maintain the pH and ionic strength during the synthesis of gels, respectively. All these chemicals were used without further purification.

2.2. Synthesis of catalysts

Copper integrated catalysts have been prepared through a modification of our previous work.[14] In a typical synthesis, amphiphilic tri-block copolymer pluronic F127 (1.00 g) was added to 27 mL 0.15 M aqueous hydrochloric acid (HCl) under vigorous stirring and was allowed to stir until dissolution. After dissolving, 2.5 g potassium chloride (KCl) was added to the mixture to balance the ionic strength of the solution. After 2 h of stirring of the mixture at room temperature, 1.3 g TVCH was added slowly into it as a co-surfactant, the system was allowed to stir overnight and a milky suspension arose. Then, it was aged for 1 day at ambient temperature and 2.33 g tetraethyl orthosilicate (TEOS) was added slowly to the micellar solution and allowed to stir for 0.5 h. Then, 0.190 g copper(I) iodide was added to that solution under vigorous stirring and the mixture was allowed to stir for another 0.5 h. After that, the mixture was covered and aged for 7 days at ambient temperature. The molar composition of the synthesis gel mixture was 1 : 0.2–0.05 : 2.99 : 0.714 : 0.006 : 1.04 : 134 for TEOS : CuO : KCl : TVCH : F127 : HCl : H_2O. The resulting solid was filtered off, washed with distilled water, and dried at 50 °C. Calcination was carried out by slowly increasing the temperature to 500 °C (1 °C min^{-1} ramping rate) and by heating at 500 °C for 5 h in the presence of air to obtain a template-free mesoporous catalyst suitable to carry out adsorption and catalytic studies. These three synthesized mesoporous copper doped silicate materials having the silica to copper ratios of 20 : 1, 10 : 1 and

5 : 1 are abbreviated as CuMSC-1, CuMSC-2 and CuMSC-3, respectively.

3. Characterization techniques

Powder X-ray diffraction patterns (XRD) of the samples were recorded on a Bruker AXS D-8 Advance diffractometer operated at 40 kV voltage and 40 mA current and calibrated with a standard silicon sample, using Ni-filtered CuKα (λ = 0.15406 nm) radiation. Transmission electron microscopic images and the semi-quantitative elemental analysis were recorded on an electron microscope Hitachi H-8100, operated at 200 kV, with a LaB_6 filament. The instrument was equipped with an energy dispersive X-ray spectroscopic (EDS) detector for light elements from ThermoNoran. The samples were first ground and dispersed in ethanol, and then evaporated over a Formvar®-coated Cu grid. SEM images (morphology of the particles) were recorded on a FEG-SEM microscope JEOL JSM-7001F operated at an accelerating voltage of 10 keV. The surface chemical composition was measured using a XPS spectrometer XSAM800 (KRATOS) operated in the fixed analyzer transmission (FAT) mode, with a pass energy of 20 eV, non-monochromatized AlKα and MgKα X-radiation ($h\nu$ = 1486.6 and 1253.6 eV, respectively) and a power of 120 W (10 mA × 12 kV). Samples were analyzed under a typical pressure in the range of 10^{-7} Pa. All sample transfers were performed in air. Samples were analyzed at room temperature, at a take-off angle relative to the surface holder (TOA) of 45°. Spectra acquisition details are as published elsewhere.[28] XPS Peak 4.1 (freeware) was used for peak fitting. As a reference for charge accumulation compensation, the C 1s binding energy for the lower BE component was set to 285 eV. For quantitative purposes, sensitivity factors were: Si 2p: 0.27; Cu $2p_{3/2}$: 4.20 and O 1s: 0.66. Nitrogen adsorption/desorption isotherms of the samples were recorded using an ASAP 2020 (Micromeritics) at 77 K. Prior to the gas adsorption measurements, the samples were degassed at 200 °C for 24 h under high vacuum. The Brunauer–Emmett–Teller (BET) specific surface area was computed using adsorption data in the relative pressure (P/P_0) range of 0.05–0.30. The pore size distribution was derived from the adsorption branch using the Barrett–Joyner–Halenda (BJH) method. The total pore volume was estimated from the amounts adsorbed at a relative pressure of 0.99. Fourier transform infrared (FT IR) spectra of these samples were recorded on KBr pellets using a Perkin-Elmer Spectrum 100 spectrophotometer. UV-visible diffuse reflectance spectra were recorded on a Shimadzu UV 2401PC with an integrating sphere attachment. $BaSO_4$ was used as the background standard.

3.1. Catalytic conditions

The catalytic oxidation reactions were carried out in Schlenk tubes fitted with a water condenser and placed in a temperature controlled oil bath under magnetic stirring. In the typical reaction, 5 wt% of CuMSC catalysts were taken with respect to substrate. Typically, 0.84 g cyclohexane was added to 6 mL acetonitrile (solvent), followed by the addition of an oxidant (H_2O_2 or TBHP, equimolar ratio with respect to the substrate) and 0.042 g catalyst. Then, the reaction was initiated with the immediate addition of 5 μL 65% HNO_3. Then, the reaction solution was allowed to stir for 5 h at the desired temperature. After completion of the catalytic reaction, 100 μL cyclopentanone was added as an internal standard and 13 mL diethyl ether was added to extract the unreacted substrate and the product(s) from the reaction mixture. The obtained organic layer was stirred for 10 minutes and then the sample was analyzed by GC using the internal standard method. The yield was estimated by comparison with known standards. The amount of alkyl hydroperoxide (if formed) was estimated from the variations in the alcohol and ketone yields, determined by GC analyses, on addition of PPh_3 to the final reaction product, according to the method reported by Shul'pin *et al.*[29] The blank reaction had been carried out without adding any catalyst, keeping other experimental conditions unchanged, and confirmed that no cyclohexanol or cyclohexanone was formed without the catalyst.

3.2. Reuse of the catalysts

At the end of the reaction, the catalyst was separated from the reaction mixture by filtration and was thoroughly washed several times with methanol, *n*-hexane and acetone to remove both non-polar and polar compounds that were adsorbed on the surface, as well as on the interior pore of the catalysts.[6b,30] After the washing, the catalysts were activated by heating them overnight at 70 °C followed by 120 °C for 4 h and then used again for the same reaction under identical reaction conditions, for recycling experiments. The whole process was repeated five times and negligible loss of the catalytic activity was observed.

4. Results and discussion

4.1. Morphological and structural characterization

The small angle powder X-ray diffraction (PXRD) patterns of the calcined mesoporous pure silicate and copper doped silicate materials are shown in Fig. 1. The material shows three well-resolved diffraction peaks in the region of 2θ = 0.68–2.0°, which can be indexed in turn to the 100, 110 and 200 reflections corresponding to two-dimensional hexagonal mesostructures with structural periodicity.[8a,14] The higher order diffraction peaks were too weak due to the incorporation of heteroatoms into the framework.[31] Pure silica shows the first diffraction peak at 0.68°, whereas after anchoring of copper into the silicate matrix, shifting of the peak occurs to the higher 2θ of 0.85° and the corresponding d spacing also reduces from 12.98 nm to 10.38 nm. The high angle PXRD patterns (Fig. 2) show no higher order diffraction peaks or characteristic peaks of CuO, indicating the amorphous nature of the pore walls.[31] Thus, it is concluded that copper might be in the framework or highly dispersed throughout the silicate surface.[13a] The slight reduction of the 100 reflections in the

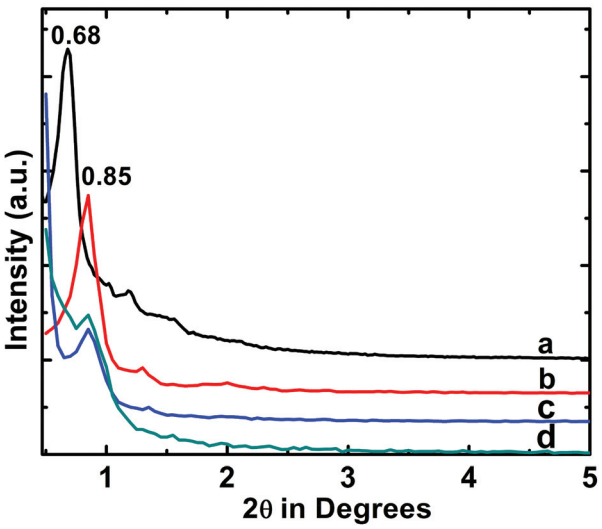

Fig. 1 Small-angle powder XRD patterns of calcined mesoporous pure silica (a), CuMSC-1 (b), CuMSC-2 (c) and CuMSC-3 (d) samples.

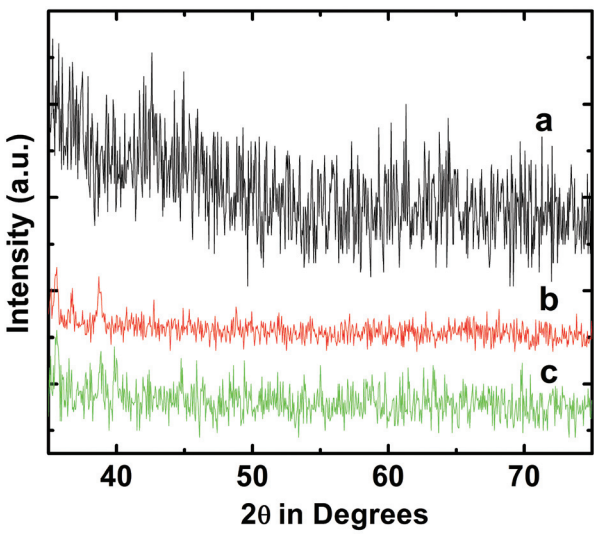

Fig. 2 Wide-angle powder XRD patterns of calcined mesoporous CuMSC-1 (a), CuMSC-2 (b) and CuMSC-3 (c) samples.

copper loaded CuMSC sample is more likely due to a dilution of silica with incorporation of copper as a consequence of its adsorption factor for X-rays being higher than the one for silicon.[32] In the literature a similar result was reported: MCM-41 was loaded with Cu up to 20 wt% but no crystalline Cu phase was observed; however, a crystalline phase was noticed in the IP gel form.[33] The small-angle PXRD of the reused CuMSC-2 sample (Fig. S1, ESI†) implies that the material keeps its porous structure after the catalytic reaction.

Representative TEM images of mesoporous CuMSC samples, shown in Fig. 3, confirm the XRD results. In these images low electron density spots (pores) are seen throughout the respective specimens. The uniform and long range ordered mesopores are clearly observed in these TEM images. TEM

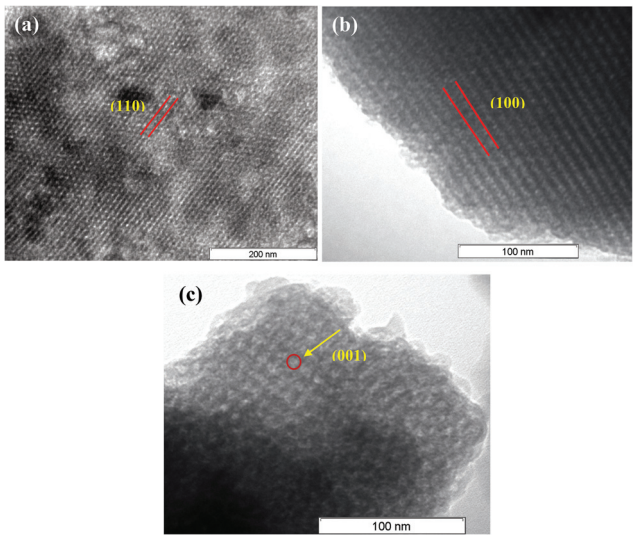

Fig. 3 TEM image of calcined mesoporous CuMSC-1 (a), CuMSC-2 (b) and CuMSC-3 (c) samples seen through the direction perpendicular to the pore axis.

recorded in the different directions indicates long range ordering and hexagonally arranged pores.[8,14] In the case of pure SBA-15 prepared by the same procedures, the observed pore size is *ca.* 9.2 nm,[14] whereas after incorporation of copper into the silica frameworks the pore size decreases to *ca.* 4.0 to 5.0 nm and the wall thickness varies from 7.0 to 8 nm. Thus, incorporation of copper into the SBA-15 silica framework makes the pore walls thicker than the pure SBA-15. Consequently, the material becomes denser.

Scanning electron microscope (SEM) images (shown in Fig. 4) reveal that calcined samples are composed of plates and a sphere-like morphology in micrometer size (Fig. 4a and 4c).

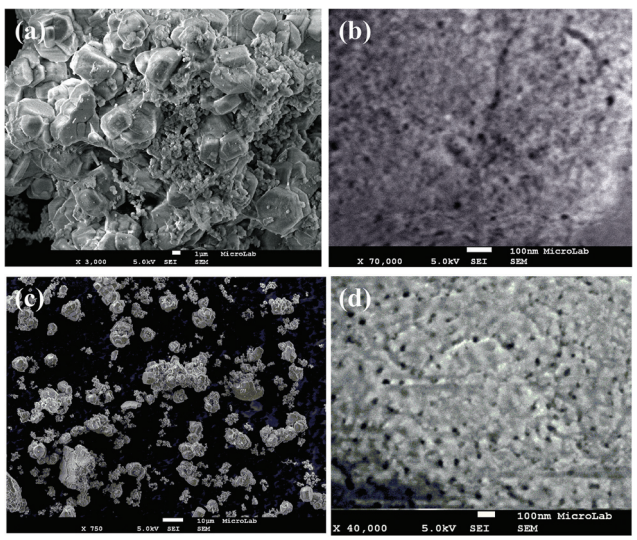

Fig. 4 FE-SEM image of calcined CuMSC-1 (a), CuMSC-1 with higher magnification (b), and CuMSC-2 (c) and CuMSC-2 with higher magnification (d).

All of these plates and spheres consist of small tiny nanoparticles that have been observed in the magnified Fig. 4b, 4d and Fig. S2 (see in ESI†). These small nanoparticles are agglomerated together to form such large sized spheres.

The nitrogen adsorption–desorption isotherms of the calcined mesoporous silica and CuMSC materials (Fig. 5) are type IV with H_2-type hysteresis loops, characteristic of capillary condensation in mesopores of undefined shapes.[9,34] The total pore volumes and the hysteresis loops decrease in the order: pure silica, CuMSC-1, CuMSC-2, and CuMSC-3. In the case of CuMSC-3, the hysteresis is so small that we may consider it type H_3, which is characteristic of slit-shaped pores or plate-like particles; this type of pore may be created due to particles aggregation (Fig. 4b, 4d; Fig. S2 in ESI†). For the pure silica matrix, the hysteresis loop is observed in the P/P_0 range of 0.50–0.80, whereas for CuMSC the P/P_0 range is 0.35–0.80. This indicates that pure silica has larger pores than the CuMSC materials. The P/P_0 position of the inflection points is clearly related to a diameter in the mesopore range, and the sharpness of these steps indicates a narrow mesopore size distribution.[35] In the case of CuMSC materials, a weak second hysteresis loop is noticed for higher P/P_0 (0.75–1.0), which indicates the presence of a poor textural mesoporosity, probably arising from noncrystalline voids and spaces generated through interparticle links.[36] The specific surface area, average pore diameter and total pore volume of these samples, derived from the respective adsorption–desorption isotherms, are summarized in Table 1. The specific surface area was estimated from the Brunauer–Emmett–Teller (BET) isotherm, the average pore diameter was derived using the BJH algorithm for the adsorption isotherms (Fig. 6), and the total pore volume from the quantity adsorbed at a single P/P_0 point (0.99). The micropore area and volume of all the samples were estimated from

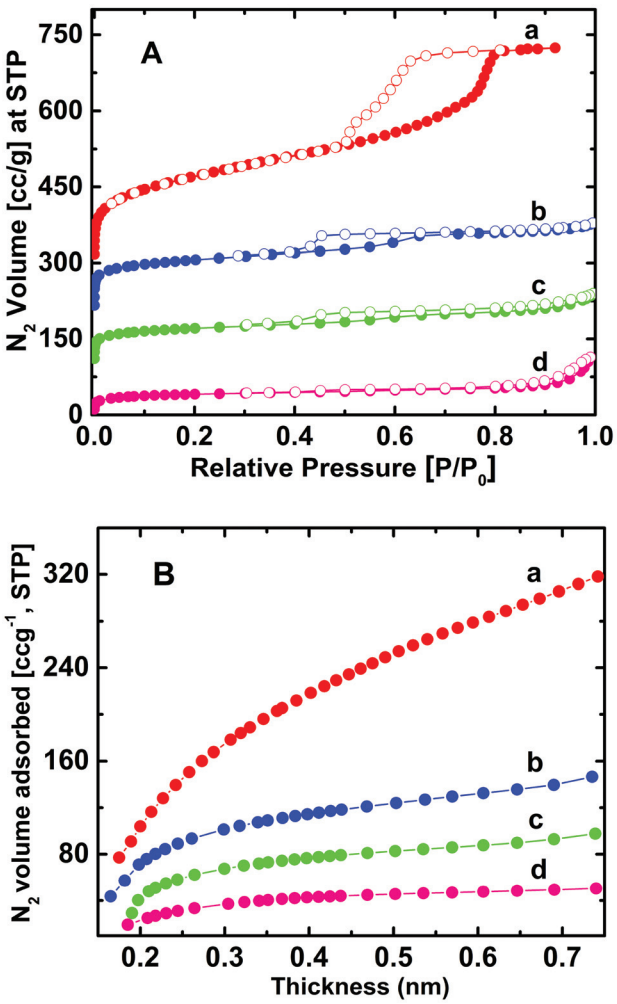

Fig. 5 (A) N_2 adsorption/desorption isotherms of mesoporous pure silica (a), CuMSC-1 (b), CuMSC-2 (c) and CuMSC-3 (d) samples, measured at 77 K. Adsorption points are marked by filled circles and desorption points by empty circles. *Y* axes of plots (a), (b) and (c) have been enhanced by 300, 200, 100 $cm^3\ g^{-1}$, respectively, for clarity. (B) t-plot analysis of mesoporous pure silica (a), CuMSC-1 (b), CuMSC-2, and CuMSC-3 (c). *Y* axes of plots (b), (c) and (d) enhanced by 30, 20, 10 $cm^3\ g^{-1}$, respectively, for clarity.

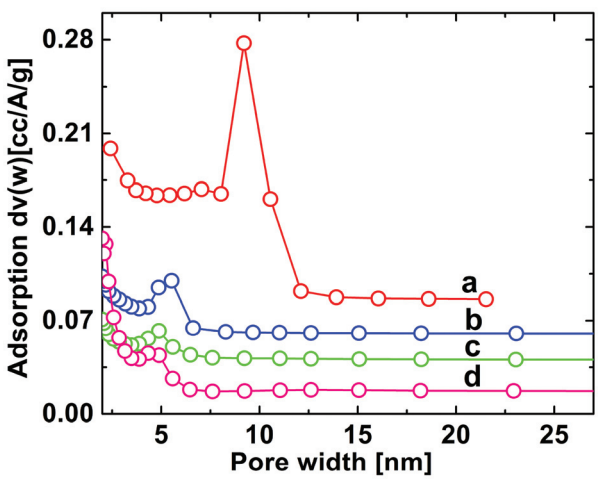

Fig. 6 BJH mesopore size distribution of pure silica (a), CuMSC-1 (b), CuMSC-2 (c) and CuMSC-3 (d).

Table 1 Physico-chemical properties of copper integrated mesoporous silicates (CuMSC)

Entry	Sample	Specific surface area/$m^2\ g^{-1}$	Pore diameter (nm)	Pore volume/$cm^3\ g^{-1}$	Micropore area/$m^2\ g^{-1}$	Micropore volume/$cm^3\ g^{-1}$
1	SBA-15	611	9.20	0.634	269	0.123
2	CuMSC-1	407	5.84	0.223	150	0.067
3	CuMSC-2	306	4.83	0.163	101	0.045
4	CuMSC-3	214	4.84	0.113	62	0.027

the *t*-plot for the adsorption isotherms (Fig. 5B) and the parameters are given in Table 1. The micropore surface area is possibly attributed to the micropores between the network hexagonal pores which are typical of SBA-15 materials. The fact that the BET surface areas of CuMSC matrices are considerably lower than that of pure silica indicates that copper incorporation into the silicate framework yields thicker pore walls, which is confirmed by the respective TEM images shown in Fig. 2. The average pore size (*ca.* 9.2 nm for pure silica and 4.0 to 5.0 nm for CuMSC materials) also agrees quite well with the pore widths obtained from the TEM images (Fig. 3) and the XRD analysis (Fig. 1).

4.2. Chemical analysis

The EDS patterns and the contents of different elements present in calcined CuMSC samples are shown in Fig. 7 and Table 2, respectively. The EDS pattern at different positions in the specimen suggested uniform distribution of Si, O and Cu in the samples and the calculation was based on the literature.[6b] The mole ratio Si : Cu has been taken as 1 : 0.05 during the gel formation for CuMSC-1, whereas after condensation and calcination the observed wt% of Si, O and Cu in the mesoporous sample was found to be 38.52, 60.33 and 1.16 wt%, respectively. Thus, the Cu : Si molar ratio in the calcined CuMSC-1 is 1 : 0.013. The molar ratio of Si : Cu has been taken as 1 : 0.1 during the gel formation for CuMSC-2, whereas after condensation and calcination the observed wt% of Si, O and Cu was found to be 34.48, 63.21 and 2.32 wt%, respectively, leading to a Si : Cu molar ratio of 1 : 0.03 in the calcined CuMSC-2. When the Si : Cu molar ratio has been taken in the gel as 1 : 0.2, the observed wt% of Si, O and Cu was found to be 36.90, 47.71 and 15.39 wt%, respectively. Thus, the estimated Si : Cu molar ratio in the calcined CuMSC-3 is 1 : 0.18. The EDS surface analysis of different elements present in the reused CuMSC-2 sample is shown in Fig. S3 and Table S1 (ESI†). From the result analysis it is clear that a very marginal decrease of copper sites happens during the catalytic progress.

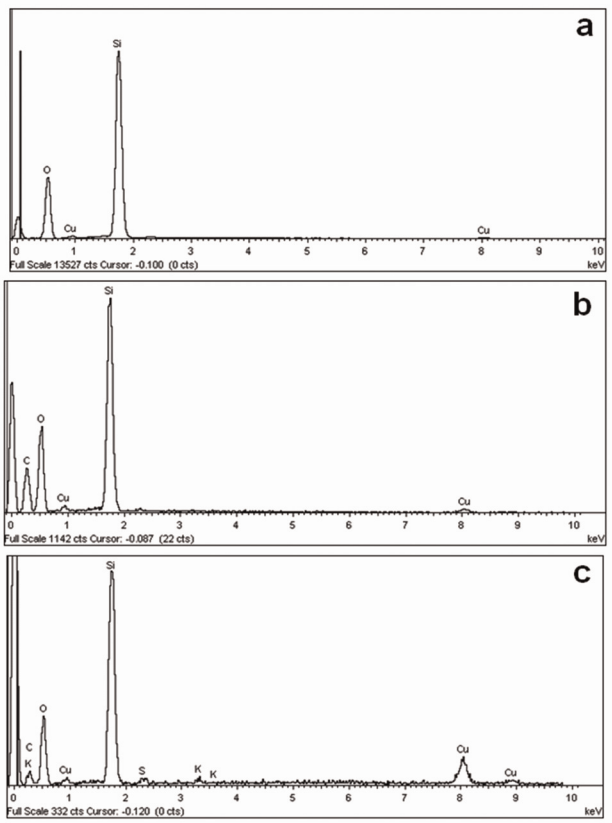

Fig. 7 EDS surface chemical analysis of calcined mesoporous CuMSC-1 (a), CuMSC-2 (b) and CuMSC-3 (c) materials.

Table 2 EDS surface chemical analysis of mesoporous CuMSC materials

Entry	Elements	keV	Weight%	Weight% error	Atomic%
CuMSC-1	O K	0.52	60.33	0.22	73.07
	Si K	1.74	38.52	0.20	26.58
	Cu K	8.05	1.16	0.18	0.35
	Total		100		100
CuMSC-2	O K	0.52	63.21	0.54	75.76
	Si K	1.74	34.48	0.49	23.54
	Cu K	8.05	2.32	0.32	0.70
	Total		100		100
CuMSC-3	O K	0.52	47.71	1.16	65.71
	Si K	1.74	36.90	0.92	28.95
	Cu K	8.05	15.39	0.88	5.34
	Total		100		100

The same samples were analyzed by XPS which gives both qualitative information about the oxidation state of elements and quantitative information concerning atomic ratios within a few nanometers depth (Fig. 8). Samples, except for CuMSC-1, were analyzed using radiation having different energies to probe different average depths in order to obtain qualitative information about distributions in-depth near the surface. MgKα radiation probes a shallower region than the AlKα one. The analyzed regions were Si 2p, Cu $2p_{3/2}$ and O1s. The Si 2p region was fit with a doublet with a spin–orbit split of 0.66 eV. The component Si $2p_{3/2}$ is centred at 103.6 ± 0.2 eV, typical of Si $2p_{3/2}$ in silica.[37] Oxygen comes mainly from the silica and could be fit with one or two components, the main one being centred at 533.0 ± 0.2 eV. Fig. 8 displays the Cu $2p_{3/2}$ region which is fittable with two (CuMSC-1 sample) or three photoelectron peaks (CuMSC-2, -3 samples) centred at 933.3 ± 0.2, 935.3 ± 0.2, 937.3 ± 0.3 eV assigned, respectively, to Cu(I), Cu(II) in CuO, and Cu(II) in $Cu(OH)_x$. The latter values are, on average, 1 eV higher than values found for the pristine copper oxides.[38] We can postulate a coordination for copper integrated in the silica framework (Scheme S1, ESI†) which does not need any further charge balance, where Cu^{2+} is coordinated by two anionic hydroxyl or siloxyl groups, as reported by others[38c] for Cu^{2+} integrated in the mesoporous silica matrix, which was applied in catalytic phenol hydroxylation. However, silanol coordination should result in acid enhancement, with eventual proton liberation. Hence, such a

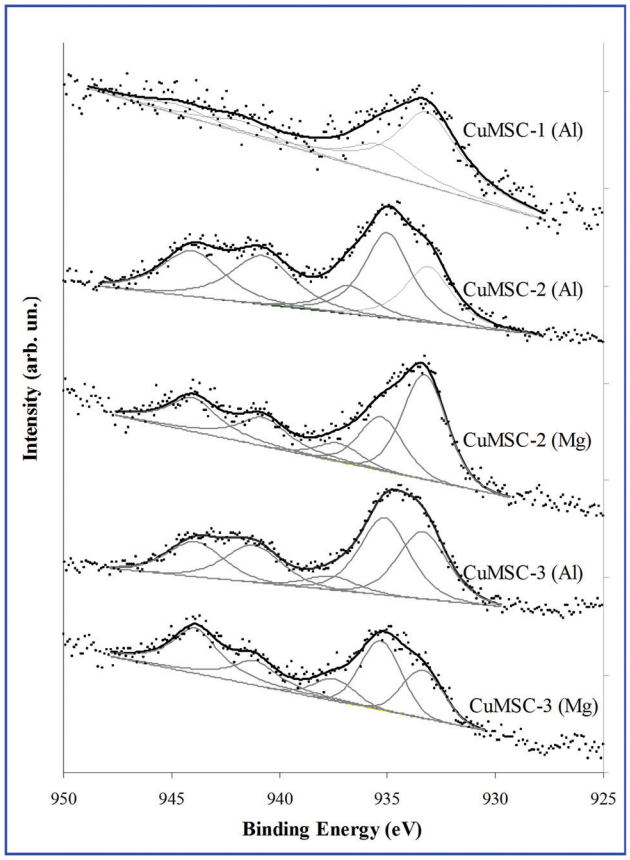

Fig. 8 XPS analysis of the Cu $2p_{3/2}$ region for the three samples.

structure model can also be viewed as ionic with protons balancing the negative charge of the copper centre with anionic deprotonated silanols. Some XPS characterizations of copper included and/or grafted specifically in SBA-15 mesoporous silica have been published attesting to the presence of copper in the form of Cu(I), Cu(II) or mixed phases of Cu(I) and Cu(II) species. In some cases, the absolute binding energies reported are not straightforwardly comparable with those presented here due to the lack of details, namely on the charge shift correction and spectra fittings and absence of XPS quantitative analysis.[39] Nevertheless, considering XPS data treatment differences and within the experimental errors, a shift of the Cu 2p region to binding energies higher than that of Cu 2p detected for bulk CuO was observed for copper doped mesoporous silica. This shift has been attributed to the incorporation of copper into the SBA-15 matrix as in Cu–O–Si structures.[39b,c,40] They generally attributed it to an initial state effect: "... indicating that the Cu atoms are surrounded by silicon in Cu-SBA-15 samples, most likely in the structure of Cu–O–Si upon incorporation of copper ions into the framework of SBA-15. The higher electron affinity of silicon causes movement of electrons from copper to silicon and then the increase in binding energy of Cu 2p".[40a] However, this is not true: the electronegativity (not the electron affinity...) of Si is very similar to the Cu one in both the Pauling[41a] and Sanderson[41b,c] scales. Other initial state causes may exist such as the coordination number. Likely, the main reason for this increase comes from a final state effect due to the lower ionic character of SiO_2 relative to copper oxides, stabilizing the final state (the inner hole resulting from the photoelectron ejection) less effectively than the more ionic oxide.[42] A study of Cu oxides deposited on SiO_2 and ZrO_2 also detected that Cu $2p_{3/2}$ binding energy increased from the bulk value typical of the respective copper oxide to larger values for decreasing loadings of Cu (where the interface had a prominent role) and that the effect was much more marked on SiO_2 than on ZrO_2.

Besides the photoelectron peaks, multiplet structures are also present, with weak intensity for the CuMSC-1 sample but very strong intensity for the other two samples. These structures are exclusively due to the paramagnetic species Cu(II) and their relative intensities correlate rather well with the relative importance of Cu(II) photoelectrons. In fact, in paramagnetic species, when an inner electron is ejected, it leaves behind an unpaired electron which may couple its spin momentum with the other (valence) unpaired electrons in several ways, giving rise to a final state with multiple spin configurations instead of a single one. Since several final states are possible, the measured binding energy of the ejected electron which reflects the difference between the charged final state and the initial state has several values.[43] Table 3 gathers the main quantitative information. The ratio Cu/Si is, within the experimental error, the same as the EDS value for the sample CuMSC-1, higher than the EDS value for CuMSC-2, but in the same order of magnitude, and much lower than the EDS value for CuMSC-3. Given the large difference of probed depth in the two analytical techniques, these differences mean that the copper

Table 3 XPS surface chemical analysis of mesoporous CuMSC materials. (Al) and (Mg) stand for the used X-ray in the measurement. MgKα radiation probes a shallower region than the AlKα one

	CuMSC-1 (Al)	CuMSC-2 (Mg)	CuMSC-2 (Al)	CuMSC-3 (Mg)	CuMSC-3 (Al)
Si[a]	25.9 ± 1.0	27.8 ± 1.0	24.5 ± 1.0	27.1 ± 1.0	25.1 ± 1.0
Cu[a]	0.44 ± 0.04	1.50 ± 0.15	1.93 ± 0.20	1.33 ± 0.15	1.45 ± 0.15
O[a]	73.6 ± 1.0	70.7 ± 1.0	73.6 ± 1.0	71.6 ± 1.0	73.5 ± 1.0
Cu/Si	0.017 ± 0.003	0.054 ± 0.008	0.079 ± 0.012	0.049 ± 0.007	0.058 ± 0.009
Cu/Si(EDS)	0.013	0.030		0.185	
Nominal Cu/Si	0.05	0.10		0.20	
Cu(II)/Cu(I)	0.4	1.0	2.0	1.9	1.4

[a] Values of all the elements present in the material are in %.

distribution is rather homogeneous in the CuMSC-1 sample but it is inhomogeneous in the rest of the samples. Moreover, since the molar ratio Cu/Si is trendily larger for larger depths ("Al" results), in both samples, near the surface, a copper concentration profile decreasing towards the extreme surface exists.

Concerning the copper oxidation state, as stated above, in all the samples some Cu(II) exists together with Cu(I). In Table 3, their relative amounts are presented. Since these amounts are computed from the area of fitted peaks, the soundness of those ratios can only be assessed by comparing these values with the multiplet/photoelectron ratio. They correlate rather well (as can be seen in Fig. 8), giving them the due support. They show that CuMSC-1 has the most part of the copper in the form of Cu(I). However, for CuMSC-2 and CuMSC-3 samples the inverse occurs. But, again, the distribution of both forms is not homogeneous in depth since the shallower ratio (Mg) is different from the deeper one (Al). It should be expectable to have the more superficial species more oxidized than the deeper ones. It is so for the CuMSC-3 sample but it is the inverse for CuMSC-2.

4.3. Optical spectroscopic studies

UV-visible spectroscopy was used to investigate the presence and the coordination mode of the metal centres in the copper integrated mesoporous silicate catalysts. In Fig. 9, the UV-vis diffuse reflectance spectra of the CuMSC materials are shown. All the spectra show a strong band at 260 nm with a smaller component at 220 nm, assigned to charge-transfer transition involving isolated framework Cu^{2+} in CuO_4 tetrahedral geometry, which suggests that some Cu^{2+} ions are incorporated into the framework of the matrix.[40a] A shoulder to higher wavelengths is poorly defined in the sample CuMSC-1, but is clear for CuMSc-3 at ~315 nm and appears as a band for the sample CuMSC-2. It is also a (LMCT, $O^{2-} \rightarrow Cu^{2+}$) charge transfer band, but in clustered CuO. The previous features confirm the existence of Cu^{2+} species, and suggest that when its bulk content is higher (CuMSC-2, as probed by XPS using AlKα radiation), it is present in two different environments: within the silica network and as clusters. Further, the DRUV spectra show a broad band at 650 nm that can be attributed to the typical d–d transition in Cu^{2+} located in a distorted octahedral or square pyramidal coordination.[7,44] This d–d transition is responsible for the green colour of the material.

FT IR spectra of the calcined pure silica and two CuMSC samples are shown in Fig. 10. The absence of bands at ~2854 and ~2925 cm^{-1}, which are ascribed to symmetric and antisymmetric vibrations of the C–H groups, indicates the complete removal of F127 molecules from all the as-synthesized materials upon calcination. The broad band at ~3500 cm^{-1} is attributed to the OH stretching mode of water and of any silanol groups and the one at 1640 cm^{-1} to the bending mode of water.[45] The large shift of the main band from 1088 (in the metal-free silicate and in CuMSC-1) to 1057 cm^{-1}, in the CuMSC-2, indicates the incorporation of copper within the silicate network and thus Si–O–Cu bonds may have formed. Generally this band corresponds to the antisymmetric Si–O–Si stretching vibration of the tetrahedral SiO_4 units.[31] It is known that the bond length of Cu–O is longer than that of Si–O, which leads to a decrease in the force constant of the bond. Furthermore, the atomic weight of Cu is higher than that of Si, so the reduced mass is increased. These factors collectively shift the vibration frequency to the lower range observed in particular for CuMSC-2. Besides, the antisymmetric Si–O–Si stretching of the doped samples has a much broader profile, which is a good indication of the silica network being deformed by incorporation of Cu. A similar effect has been reported on Cu doped TiO_2 nanoparticles.[46] The silanol groups are in very low concentration, because the Si–OH stretch expected at ~950 cm^{-1} is not resolved from the main silica band in all the samples. Confirmation of the existence of Cu–O bonds in the sample CuMSC-2 comes from the small

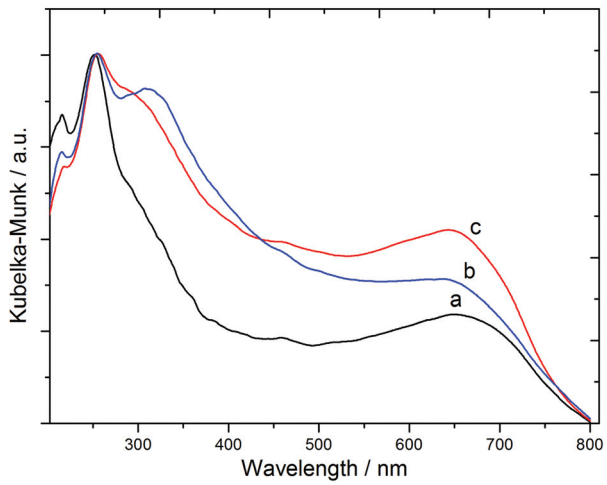

Fig. 9 UV-vis reflectance spectra of CuMSC-1 (a), CuMSC-2 (b) and CuMSC-3 (c), normalized to the maximum absorption.

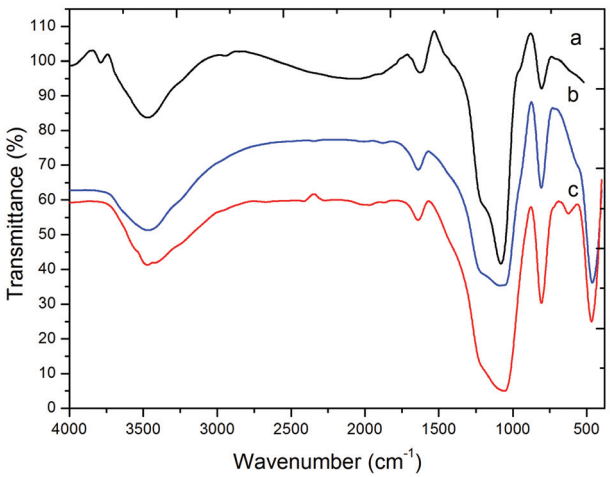

Fig. 10 FT IR spectra of pure silicate (a), CuMSC-1 (b) and CuMSC-2 (c), normalized to the maximum transmittance.

band that appears at 621 cm^{-1} assigned to the Cu–O stretching vibration.[47]

5. Catalytic reaction

The catalytic oxidation of cyclohexane with H_2O_2 as an oxidant has been carried out heterogeneously by using the copper integrated mesoporous silicate catalysts with different n_{Si}/n_{Cu} ratios, at different temperatures (Scheme 1). Acetonitrile was used as the solvent for the liquid phase. In all the cases, cyclohexanone is the major product (selectivity usually above 70%) and cyclohexanol is formed in smaller amounts. The results of catalytic activities of the CuMSC are shown in Table 4. In view of the good catalytic activity, a low catalyst load was used, typically 5 wt% catalyst with respect to cyclohexane, leading to a maximum overall (cyclohexanone and cyclohexanol) yield of 29% for the CuMSC-2 catalyst (n_{Si}/n_{Cu} molar ratio of 35) with a total TON of 230 (Table 4, entry 2), at 50 °C, after 5 h reaction time. An increase of n_{Si}/n_{Cu} to 75 (CuMSC-1), corresponding to a decrease of the integrated copper in the matrix, leads to a lowering of yield to 17% but with an enhancement of TON to 276 (Table 4, entry 1). For CuMSC-3 with the highest copper integration (n_{Si}/n_{Cu} is 5.5), the lowest TON was obtained (Table 4, entries 3, 6 and 9). When the copper content in the CuMSC materials is excessive, the deposited CuO covers some of the active copper sites and blocks the pore interior, thus hampering the access to the active catalytic sites.[18] These factors result in a decrease of the catalytic activity of CuMSC-3. Moreover, CuMSC-1, with the lowest copper content, leads to the lowest product yield due to the lowest amount of active sites. It is interesting to notice that the catalytic activity as a function of the nominal composition of the catalyst follows the same trend as the XPS Cu/Si %, demonstrating that the active sites at the extreme surface are the important ones for the catalysis. This results from the greater accessibility of these sites. We have considered all the Cu sites as the active sites and based on that we estimated the catalytic activity. Actually this is the apparent activity. Basically, for this type of solid matrix with doped active sites, it is very difficult to find out the exact number of active sites and regarding this difficulty we usually calculate the activity by taking such an approach.

Temperature is a relevant factor, and *e.g.*, lowering to 30 °C (Table 4, entries 4–6), in the case of CuMSC-2, results in decreasing the overall yield to 18% and the overall TON to 140 (Table 4, entry 5). The presence of acid (HNO_3) is also important, and when the reaction is undertaken in its absence (entries 7–10), the yield and TON lower markedly, *e.g.*, to 6.5% and 52, respectively, when using CuMSC-2 (entry 8). In this reaction, a slight amount of nitric acid plays a vital role enhancing the total yield in the catalysis. This is probably due to the following: (i) enhancement of the oxidative properties of the active metal centres; (ii) oxidation of Cu(I) (either initially present in the framework or generated in the catalytic cycle);[23f] (iii) hampering the decomposition of H_2O_2 into water and oxygen, and promoting peroxo (or hydroperoxo)-complexes formation and its stabilization as well;[23a,c,f] (iv) promoting proton-shifts which play an important role in the metal catalyzed hydroxyl radical generation from H_2O_2.[23g,h]

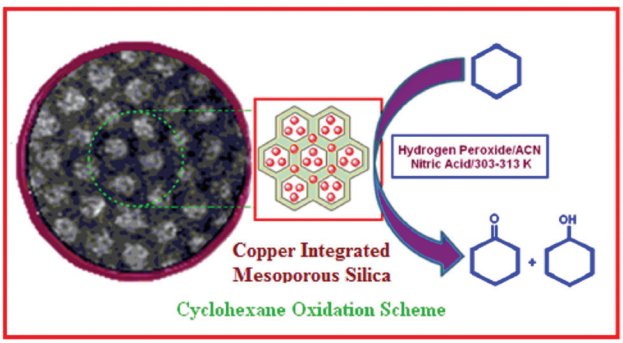

Scheme 1 Schematic representation for the oxidation reactions by a copper integrated mesoporous silicate catalyst (CuMSC).

Table 4 Cyclohexane oxidation by copper integrated mesoporous silica catalysts (CuMSC)[a]

			Yield (%)			Selectivity (%)		TON[b]		
Entry	Catalyst	Temp. (°C)	$C_6H_{10}O$	$C_6H_{11}OH$	Total yield (%)	$C_6H_{10}O$	$C_6H_{11}OH$	$C_6H_{10}O$	$C_6H_{11}OH$	Total TON
1	CuMSC-1	50	12.5	4.4	16.9	73.9	26.1	204	72	276
2	CuMSC-2	50	20.6	8.3	29.0	71.0	29.0	164	66	230
3	CuMSC-3	50	13.3	7.0	20.8	63.9	34.1	17	9	26
4	CuMSC-1	30	9.1	3.4	12.5	72.8	27.2	148	55	203
5	CuMSC-2	30	12.4	5.2	17.6	70.5	29.5	99	41	140
6	CuMSC-3	30	9.8	4.5	14.3	68.5	31.5	12	6	18
7[c]	CuMSC-1	50	5.5	1.5	7.0	78.6	21.4	90	24	114
8[c]	CuMSC-2	50	5.6	1.7	7.3	76.7	23.6	45	14	59
9[c]	CuMSC-3	50	3.9	2.1	6.0	65.0	35.0	5	3	8
10[c]	CuMSC-2	30	4.2	2.3	6.5	75.5	24.5	34	18	52
11[d]	CuMSC-2	50	3.4	1.8	5.2	65.4	34.6	27	14	41
12[e]	—	50	1.0	0.5	1.5	66.7	33.3	—	—	—

[a] Conditions, unless stated otherwise: 5 wt% catalyst (42 mg), 10 mmol (0.84 g) cyclohexane, 6 mL acetonitrile, H_2O_2 (1 : 1 mole ratio relative to cyclohexane), HNO_3 (5 μL, 65%), 5 h reaction time. [b] TON (turnover number) = moles of product/mole of active sites (dispersed Cu-sites) of catalyst. [c] Without HNO_3. [d] Using TBHP instead of H_2O_2 in the presence of HNO_3. [e] In the absence of catalyst.

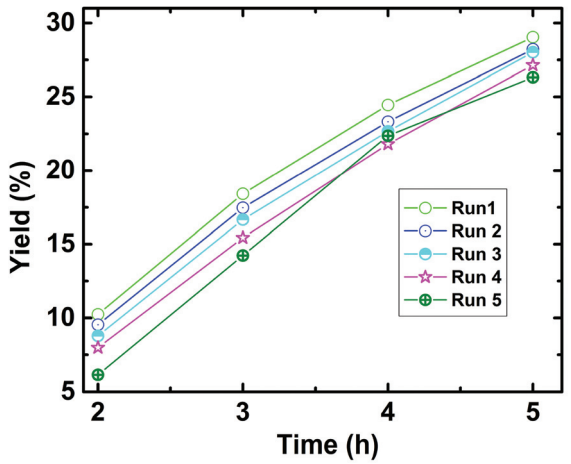

Fig. 11 Kinetic curves of product yields in various runs with respect to time, upon catalyst recycling for cyclohexane oxidation by using CuMSC-2.

The use of H_2O_2 as an oxidizing agent is potentially significant from an environmental viewpoint (water is the only by-product and decomposition leads also to the formation of O_2).[23a] Replacement of H_2O_2 by *tert*-butyl hydrogen peroxide (TBHP) leads to a dramatic decrease of the activity (5% yield, for CuMSC-2, in the presence of HNO_3, entry 10, Table 4). Blank experiments confirmed that the cyclohexane oxidation does not occur considerably in the absence of the CuMSC catalyst (entry 11, Table 4).

The stability of the CuMSC, as well as the heterogeneous nature of the catalysis, was tested as follows. Hot filtration of a solution of the CuMSC-2 catalyst under the optimized reaction conditions allowed the separation of the solid catalyst which was recycled with fresh reagents upon applying the same reaction conditions and no loss of its catalytic activity was observed. Moreover, the filtered solution upon addition of more H_2O_2 did not show activity for the cyclohexane oxidation. These results indicate that during the reaction no appreciable catalyst leaching occurs and the reaction is essentially heterogeneous. The activity of a regenerated catalyst was inspected upon separation, by filtration, of the solid catalyst from the reaction mixture and then washing several times with methanol, *n*-hexane and dried acetone, followed by drying in an oven at 70 °C overnight. The catalyst was subsequently activated at 120 °C for 4 h under air flow and utilized for the above reaction. The kinetics (yield *versus* reaction time) concerning the various recycles (up to five times) were studied under similar reaction conditions, as shown in Fig. 11, whereas the final yields of the catalytic recycles are given in Fig. S4 (see ESI†). No marked loss of catalytic activity is observed.

6. Conclusions

In conclusion, we have presented a new, simple and convenient synthetic strategy for the preparation of copper functionalized mesoporous silica from commercially available sources. Combination of a triblock copolymer, pluronic F127, and TVCH generates an ordered mesoporous architecture. TEM and N_2 adsorption/desorption studies established the mesoporous nature of these materials which have been thoroughly characterized using PXRD, FEG-SEM, FT-IR, XPS and diffuse reflectance UV-Vis spectroscopy. The green colour of the compound is due to d–d transitions and this has been revealed from UV-visible reflectance spectroscopy. XPS analysis detects the divalent and monovalent oxidation state of the copper atom. The successful incorporation of copper into the 2D-hexagonal silicate framework, as well as the high surface area and uniform mesopores, have conferred to the material a good catalytic activity for cyclohexane oxidation, as demonstrated herein. Moreover, this mesoporous solid catalyst has been recycled five times with a negligible loss of activity, a feature of high catalytic importance.

Acknowledgements

This work was partially supported by the Fundação para a Ciência e a Tecnologia (FCT), Portugal (projects PTDC/QUI-QUI/102150/2008, PEst-OE/OUI/UI0100/2013 and PEst-OE/CTM/LA0024/2011). S. K. D. (grant no. SFRH/BPD/74626/2010) and S. M. (grant no. SFRH/BPD/43764/2008) also wish to express gratitude to the FCT for postdoctoral fellowships, and L. M. F. Lopes acknowledges FCT for PhD grant SFRH/BD/62616/2009.

References

1 (*a*) C. T. Kresge, M. E. Leonowicz, W. J. Roth, J. C. Vartuli and J. S. Beck, *Nature*, 1992, **359**, 710–712; (*b*) J. S. Beck, J. C. Vartuli, W. J. Roth, M. E. Leonowicz, C. T. Kresge, K. D. Schmitt, C. T. W. Chu, D. H. Olson, E. W. Sheppard, S. B. McCullen, J. B. Higgins and J. L. Schlenke, *J. Am. Chem. Soc.*, 1992, **114**, 10834–11084.

2 (*a*) A. I. Acatrinei, M. A. Hartl, J. Eckert, E. H. L. Falcao and C. L. L. Daemen, *J. Phys. Chem. C*, 2009, **113**, 15634–15638; (*b*) B. Zheng, Z. Yang, J. Bai, Y. Lia and S. Li, *Chem. Commun.*, 2012, **48**, 7025–7027.

3 (*a*) A. K. Sinha and K. Suzuki, *Angew. Chem., Int. Ed.*, 2005, **44**, 271–273; (*b*) H. Park, S. H. Yang, Y.-S. Jun, W. H. Hong and J. K. Kang, *Chem. Mater.*, 2007, **19**, 535–542; (*c*) D. Chandra, S. K. Das and A. Bhaumik, *Microporous Mesoporous Mater.*, 2010, **128**, 34–40; (*d*) Y. Liu, D. Liu, Q. Yang, C. Zhong and J. Mi, *Ind. Eng. Chem. Res.*, 2010, **49**, 2902–2906.

4 T. Waitz, T. Wagner, T. Sauerwald, C.-D. Kohl and M. Tiemann, *Adv. Funct. Mater.*, 2009, **19**, 653–661.

5 A. Corma, P. Atienzar, H. Garcia and J.-Y. Chane-Ching, *Nature*, 2004, **3**, 394.

6 (*a*) J. H. Clark, D. J. Macquarrie and S. J. Tavener, *Dalton Trans.*, 2006, 4297–4309; (*b*) S. K. Das, M. K. Bhunia,

A. K. Sinha and A. Bhaumik, *ACS Catal.*, 2011, **1**, 493–501; (*c*) T. Sen, J. Whittle and M. Howard, *Chem. Commun.*, 2012, **48**, 4232–4234.

7 M. Nandi, P. Roy, H. Uyama and A. Bhaumik, *Dalton Trans.*, 2011, **40**, 12510–12518.

8 (*a*) D. Zhao, J. Feng, Q. Huo, N. Melosh, G. H. Fredrickson, B. F. Chmelka and G. D. Stucky, *Science*, 1998, **279**, 548–552; (*b*) J. Jarupatrakorn and T. D. Tilley, *J. Am. Chem. Soc.*, 2002, **124**, 8380–8388.

9 (*a*) Y. M. Liu, Y. Cao, K. K. Zhu, S. R. Yan, W. L. Dai, H. Y. He and K. N. Fan, *Chem. Commun.*, 2002, 2832–2833; (*b*) Y. M. Liu, Y. Cao, N. Yi, W. L. Feng, S. R. Yan, W. L. Dai, H. Y. He and K. N. Fan, *J. Catal.*, 2004, **224**, 417–428.

10 A. Taguchi and F. Schüth, *Microporous Mesoporous Mater.*, 2005, **77**, 1–45.

11 B. Jarry, F. Launay, J. P. Nogier, V. Montouillout, L. Gengembre and J. L. Bonardet, *Appl. Catal., A*, 2006, **309**, 177–186.

12 (*a*) K. Iwanami, J.-C. Choi, B. Lu, T. Sakakura and H. Yasuda, *Chem. Commun.*, 2008, 1002–1004; (*b*) S. K. Das, M. K. Bhunia and A. Bhaumik, *Open Catal. J.*, 2012, **5**, 56–65.

13 (*a*) Y. Li, Z. C. Feng, Y. X. Lian, K. Q. Sun, L. Zhang, G. Q. Jia, Q. H. Yang and C. Li, *Microporous Mesoporous Mater.*, 2005, **84**, 41–49; (*b*) C. Nozaki, C. G. Lugmair, A. T. Bell and T. D. Tilley, *J. Am. Chem. Soc.*, 2002, **124**, 13194–13203; (*c*) A. Vinu, D. P. Sawant, K. Ariga, K. Z. Hossain, S. B. Halligudi, M. Hartmann and M. Nomura, *Chem. Mater.*, 2005, **17**, 5339–5345.

14 S. K. Das, M. K. Bhunia and A. Bhaumik, *J. Solid State Chem.*, 2010, **183**, 1326–1333.

15 C. K. Krishnan, T. Hayashi and M. Ogura, *Adv. Mater.*, 2008, **20**, 2131–2136.

16 (*a*) X. Wang, Q. Zhang, Q. Guo, Y. Lou, L. Yang and Y. Wang, *Chem. Commun.*, 2004, 1396; (*b*) E. Byambajav and Y. Ohtsuka, *Appl. Catal., A*, 2003, **252**, 193–204.

17 R. Murugavel and H. W. Roesky, *Angew. Chem., Int. Ed.*, 1997, **109**, 477–479.

18 (*a*) C. M. Chanquía, L. Andrini, J. D. Fernández, M. E. Crivello, F. G. Requejo, E. R. Herrero and G. A. Eimer, *J. Phys. Chem. C*, 2010, **114**, 12221–12229; (*b*) Y. Li, D. An, Q. Zhang and Y. Wang, *J. Phys. Chem. C*, 2008, **112**, 13700–13708.

19 (*a*) X. Guo, M. Lai, Y. Kong, W. Ding and Q. Yan, *Langmuir*, 2004, **20**, 2879–2882; (*b*) M. W. E. van den Berg, S. Polarz, O. P. Tkachenko, K. V. Klementiev, M. Bandyopadhyay, L. Khodeir, H. Gies, M. Muhler and W. Grünert, *J. Catal.*, 2006, **241**, 446–455.

20 J. Mondal, A. Modak, A. Dutta, S. Basu, S. N. Jha, D. Bhattacharyya and A. Bhaumik, *Chem. Commun.*, 2012, **48**, 8000–8002.

21 (*a*) *Ullmann's Encyclopedia of Industrial Chemistry*, Wiley-VCH, Weinheim, 6th edn, 2002; (*b*) W. Weissermel and H. J. Horpe, *Industrial Organic Chemistry*, VCH, Weinheim, 2nd edn, 1993.

22 (*a*) S. Shylesh, P. S. Prinson and A. Singh, *Appl. Catal., A*, 2007, **318**, 128–136; (*b*) H.-X. Yuan, Q.-H. Xia, H.-J. Zhan, X.-H. Lu and K.-X. Su, *Appl. Catal., A*, 2006, **304**, 178–184.

23 (*a*) T. F. S. Silva, E. C. B. A. Alegria, L. M. D. R. S. Martins and A. J. L. Pombeiro, *Adv. Synth. Catal.*, 2008, **350**, 706–716; (*b*) M. Vennat, P. Herson, J. M. Bregeault and G. B. Shul'pin, *Eur. J. Inorg. Chem.*, 2003, 908–917; (*c*) T. F. S. Silva, G. S. Mishra, M. F. G. da Silva, R. Wanke, L. M. D. R. S. Martins and A. J. L. Pombeiro, *Dalton Trans.*, 2009, 9207–9215; (*d*) R. R. Fernandes, J. Lasri, A. M. Kirillov, M. F. C. G. da Silva, J. A. L. da Silva, J. J. R. F. da Silva and A. J. L. Pombeiro, *Eur. J. Inorg. Chem.*, 2011, 3781–3790; (*e*) K. R. Gruenwald, A. M. Kirillov, M. Haukka, J. Sanchiz and A. J. L. Pombeiro, *Dalton Trans.*, 2009, 2109–2120; (*f*) M. Nandi and P. Roy, *Indian J. Chem., Sect. A: Inorg., Bio-inorg., Phys., Theor. Anal. Chem.*, 2013, 1263–1268; (*g*) M. V. Kirillova, Y. N. Kozlov, L. S. Shul'pina, O. Y. Lyakin, A. M. Kirillov, E. P. Talsi, A. J. L. Pombeiro and G. B. Shul'pin, *J. Catal.*, 2009, **268**, 26–38; (*h*) M. Kuznetsov and A. J. L. Pombeiro, *Inorg. Chem.*, 2009, **48**, 307–318.

24 (*a*) L. C. Gregor, G. T. Rowe, E. Rybak-Akimova and J. P. Caradonna, *Dalton Trans.*, 2012, **41**, 777–782; (*b*) M. N. Kopylovich, A. C. C. Nunes, K. T. Mahmudov, M. Haukka, T. C. O. Mac Leod, L. M. D. R. S. Martins, M. L. Kuznetsov and A. J. L. Pombeiro, *Dalton Trans.*, 2011, **40**, 2822–2836; (*c*) U. Schuchardta, D. Cardoso, R. Sercheli, R. Pereira, R. S. da Cruz, M. C. Guerreiro, D. Mandelli, E. V. Spinacé and E. L. Pires, *Appl. Catal., A*, 2001, **211**, 1–17; (*d*) T. C. O. M. Leoda, M. N. Kopylovich, M. F. C. G. da Silva, K. T. Mahmudov and A. J. L. Pombeiro, *Appl. Catal., A*, 2012, **439–440**, 15–23; (*e*) D. S. Nesterov, V. N. Kokozay, V. V. Dyakonenko, O. V. Shishkin, J. Jezierska, A. Ozarowski, A. M. Kirillov, M. N. Kopylovich and A. J. L. Pombeiro, *Chem. Commun.*, 2006, 4605–4607; (*f*) K. T. Mahmudov, M. N. Kopylovich, M. F. C. G. da Silva, P. J. Figiel, Y. Y. Karabach and A. J. L. Pombeiroa, *J. Mol. Catal. A: Chem.*, 2010, **318**, 44–50.

25 (*a*) G. Lü, R. Zhao, G. Qian, Y. Qi, X. Wang and J. Suo, *Catal. Lett.*, 2004, **97**, 115–118; (*b*) J. Li, Y. Shi, L. Xu and G. Lu, *Ind. Eng. Chem. Res.*, 2010, **49**, 5392–5399.

26 P. Wu, Z. Xiong, K. P. Loh and X. S. Zhao, *Catal. Sci. Technol.*, 2011, **1**, 285–294.

27 M. K. Bhunia, S. K. Das, P. Pachfule, R. Banerjee and A. Bhaumik, *Dalton Trans.*, 2012, **41**, 1304–1311.

28 A. M. Ferraria, J. D. Lopes da Silva and A. M. Botelho do Rego, *Polymer*, 2003, **44**, 7241–7249.

29 (*a*) G. B. Shul'pin, G. Suss-Fink and J. R. L. Smith, *Tetrahedron*, 1999, **55**, 5345; (*b*) G. B. Shul'pin, *J. Mol. Catal. A: Chem.*, 2002, **189**, 39–66; (*c*) G. B. Shul'pin, *C. R. Chim.*, 2003, **6**, 163–178.

30 K. Jacobson, R. Gopinath, L. C. Meher and A. K. Dalai, *Appl. Catal., B*, 2008, **85**, 86–91.

31 C. Wu, Y. Kong, F. Gao, Y. Wu, Y. Lu, J. Wang and L. Dong, *Microporous Mesoporous Mater.*, 2008, **113**, 163–170.

32 B. Solsona, T. Blasco, J. M. L. Nieto, M. L. Peña, F. Rey and A. Vidal-Moya, *J. Catal.*, 2001, **203**, 443–452.

33 X. Guo, M. Lai, Y. Kong, W. Ding and Q. Yan, *Langmuir*, 2004, **20**, 2879–2882.

34 (*a*) W. Yue, A. H. Hill, A. Harrison and W. Zhou, *Chem. Commun.*, 2007, 2518; (*b*) S. K. Das, M. K. Bhunia and A. Bhaumik, *Dalton Trans.*, 2010, **39**, 4382–4390.

35 C. Jin, G. Li, X. Wang, L. Zhao, L. Liu, H. Haiou, L. Liu, W. Zhang, X. Han and X. Bao, *Chem. Mater.*, 2007, **19**, 1664–1670.

36 M. A. Karakassides, K. G. Fournaris, A. Travlos and D. Petridis, *Adv. Mater.*, 1998, **10**, 483–486.

37 R. Cabeça, V. Martins, A. M. Ferraria, A. M. Botelho do Rego, P. Brogueira, D. M. F. Prazeres, L. P. Fonseca, V. Chu and J. P. Conde, *Sens. Actuators, B*, 2010, **149**, 432–438.

38 (*a*) G. Lavareda, C. Nunes de Carvalho, A. M. Ferraria, A. M. Botelho do Rego and A. Amaral, *J. Nanosci. Nanotechnol.*, 2012, **12**, 6754–6757; (*b*) M. T. Marques, A. M. Ferraria, J. B. Correia, A. M. Botelho do Rego and R. Vilar, *Mater. Chem. Phys.*, 2008, **109**, 174–180; (*c*) G. Zhang, J. Long, X. Wang, W. Dai, Z. Li, L. Wu and X. Fu, *New J. Chem.*, 2009, **33**, 2044–2050.

39 (*a*) H. Li, M. Yang, X. Zhang, L. Yan, J. Li and Y. Qi, *New J. Chem.*, 2013, **37**, 1343–1349; (*b*) J. Gu, Y. Huang, S. P. Elangovan, Y. Li, W. Zhao, I. Toshio, Y. Yamazaki and J. Shi, *J. Phys. Chem. C*, 2011, **115**, 21211–21217; (*c*) A. G. Kong, W. H. Wang, X. Yang, Y. W. Hou and Y. K. Shan, *Microporous Mesoporous Mater.*, 2009, **118**, 348–353; (*d*) D. An, Q. Zhang and Y. Wang, *Catal. Today*, 2010, **157**, 143–148.

40 (*a*) H. Zhang, C. Tang, Y. Lv, C. Sun, F. Gao, L. Dong and Y. Chen, *J. Colloid Interface Sci.*, 2012, **380**, 16–24; (*b*) T. Tsoncheva, V. D. Santo, A. Gallo, N. Scotti, M. Dimitrov and D. Kovacheva, *Appl. Catal., A*, 2011, **406**, 13–21.

41 (*a*) L. Pauling, *J. Am. Chem. Soc.*, 1932, **54**(9), 3570–3582; (*b*) Sanderson scales, R. T. Sanderson, *Chemical bond and bond energy*, Academic, New York, 2nd edn, 1976; (*c*) R. T. Sanderson, *J. Am. Chem. Soc.*, 1983, **105**, 2259–2261.

42 J. P. Espinós, J. Morales, A. Barranco, A. Caballero, J. P. Holgado and A. R. González-Elipe, *J. Phys. Chem. B*, 2002, **106**, 6921–6929.

43 (*a*) J. Ghijsen, L. H. Tjeng, J. van Elp, H. Eskes, J. Westerink and G. A. Sawatzky, *Phys. Rev. B: Condens. Matter*, 1988, **38**, 11322–11330; (*b*) *Surface Analysis by Auger and X-ray Photoelectron Spectroscopy*, ed. D. Briggs, J. T. Grant, IM Publications and Surface Spectra Limited, Trowbridge, 2003, pp. 438–439.

44 (*a*) R. S. da Cruza, J. M. de S. e Silva, U. Arnold, M. S. Sercheli and U. Schuchardt, *J. Braz. Chem. Soc.*, 2002, **13**, 170–176; (*b*) Y. Kong, H. Zhu, G. Yang, X. Guo, W. Hou, Q. Yan, M. Gu and C. Hu, *Adv. Funct. Mater.*, 2004, **14**, 816–820.

45 (*a*) Y. Nishiyama, S. Tanaka, H. W. Hillhouse, N. Nishiyama, Y. Egashira and K. Ueyama, *Langmuir*, 2006, **22**, 9469–9472; (*b*) S. K. Das, M. K. Bhunia, M. M. Seikh, S. Dutta and A. Bhaumik, *Dalton Trans.*, 2011, **40**, 2932–2939.

46 B. Choudhury, M. Dey and A. Choudhury, *Int. Nano Lett.*, 2013, **3**, 25.

47 M. S. Soylu, O. Z. Yeşilel, B. Karabulut and O. Büyükgüngörin, *Polyhedron*, 2009, **28**, 2487–2493.

